]www.sciencemag.org/cgi/content/full/321/5889/676/DC1

Supporting Online Material for

Colossal Ionic Conductivity at Interfaces of Epitaxial ZrO_2:Y_2O_3/$SrTiO_3$ Heterostructures

J. Garcia-Barriocanal, A. Rivera-Calzada, M. Varela, Z. Sefrioui, E. Iborra, C. Leon, S. J. Pennycook, J. Santamaria*

*To whom correspondence should be addressed. E-mail: jacsan@fis.ucm.es

Published 1 August 2008, *Science* **321**, 676 (2008)
DOI: 10.1126/science.1156393

This PDF file includes:

Materials and Methods
SOM Text
Figs. S1 to S3
References

Supporting Online Material

Colossal Ionic Conductivity At Interfaces Of Epitaxial ZrO_2:Y_2O_3 /$SrTiO_3$ Heterostructures

J. Garcia-Barriocanal,[1] A. Rivera-Calzada,[1] M. Varela,[2] Z. Sefrioui,[1] E. Iborra,[3] C. Leon,[1] S. J. Pennycook,[2] J. Santamaria[1]

[1]GFMC, Universidad Complutense de Madrid, Madrid 28040, Spain
[2]Materials Science & Technology Division, Oak Ridge National Laboratory, Oak Ridge, TN 37831, USA
[3]Escuela Técnica Superior de Ingenieros de Telecomunicaciones. Universidad Politécnica de Madrid. Madrid 28040, Spain.

MATERIALS AND METHODS

8 mol% $(Y_2O_3)_x$ $(ZrO_2)_{1-x}$ (YSZ) and $SrTiO_3$ (STO) layers were grown on STO (100) substrates in a high pressure (3 mbar) pure oxygen RF sputtering system. High pressure and high substrate temperature (900 ºC) ensures a slow (1 nm/min) and highly thermalized growth of complex oxides providing excellent epitaxial properties (S1, S2). STO / YSZ / STO trilayers were grown keeping the STO thickness constant at 10 nm or 25 unit cells (u. c.), and systematically varying the YSZ thickness in the following steps: 1, 5, 30, and 62 nm (2, 10, 60, 120 u. c. respectively). Superlattices were also fabricated, with several YSZ thicknesses, and 10 nm of STO, repeated different times (between 2 and 20).

The structure was analyzed by x-ray diffraction (XRD) in a Philips MRD X'pert, using a Cu cathode as an x-ray source. In figure S1 a typical high angle (θ -2θ) XRD pattern is plotted of a $[YSZ_{1nm}/ STO_{10nm}]_{20}$ superlattice. The artificial modulation of the superlattice provides a feature rich diffraction plot which is very amenable for roughness evaluation. Note the narrow peaks shown in figure S1, and the high number of satellite peaks observed in a broad range of the spectra around the main superlattice peaks. The XRD pattern of figure S1 indicates the coherent growth of the sample along

the *c* direction. The inset of figure S1 shows the low angle reflectivity XRD spectra of the same superlattice, where superlattice peaks due to the different refraction index of both materials are observed up to 8º. The superlattice lateral coherence length, calculated from the width of the superlattice Bragg peaks, was found to be around 100 nm. Therefore, structural coherence is limited by sample thickness in the growth direction although it may be longer in the lateral dimension.

Sample structure was also probed by scanning transmission electron microscopy (STEM). Z-contrast images were obtained in a VG Microscopes HB501UX operated at 100 kV and a HB603UX STEM operated at 300 kV, both of them equipped with Nion aberration correctors and with cold field emission guns. The VG501 has a Gatan Enfina electron energy loss spectrometer (all of the EELS data presented here were acquired in this column). Cross section samples for STEM were prepared by conventional grinding, dimpling and ion milling with Ar ions with an energy of 5 kV, at an incidence angle of 6º. Final cleaning was done at a low voltage of 0.5 kV. Regarding figure 4A, the EELS analysis of Sr M_3 (dark yellow) and the Ti $L_{2,3}$ (red) absorption lines was performed subtracting the background from the raw EEL spectra using a power law fit. Then, the edge intensity was integrated using a 10 eV wide window. Such integrated intensities were averaged and normalized to the intensity across the first complete layer (located approximately between 2.5 and 12.5 nm).

Lateral conductivity measurements in the frequency range 20 Hz - 1 MHz and at temperatures between 300 K and 673 K were performed in a 4284A (Agilent) precision LCR meter, using a four-terminal pair measurement configuration which allows stable and accurate measurements in the whole frequency range. This method avoids the measurement limitations inherent to mutual inductance, interference of the measurement signals, and unwanted residual factors arising in an ordinary termination (two terminals) method which may have significant effects at high frequency. We have set a voltage signal level of 0.5 V which corresponds to an electric field of 1 V/cm. The conductance of our samples ranges from 10 nS to 10 μS, values which are not particularly low considering that the specified measuring range of the instrument extends down to 0.01 nS. The relative accuracy is comprised between 0.1 and 0.25% in the whole frequency and conductance range.

Samples were placed in a quartz cell and were measured under air and nitrogen atmospheres and the same conductivity values were obtained, showing a negligible dependence on partial oxygen pressure. Electrodes were evaporated silver pads on top

to which leads were attached by using Ag paste. Measurements done with other electrodes like Ti-Mo alloy or Au yielded the same conductivity values thus ruling out problems related to possible Ag diffusivity.

Test samples with buried metallic contacts defined by ion milling showed very similar conductance values indicating that current flows parallel to the layers. To obtain the conductivity, the measured conductance was multiplied by a geometric factor given by the ratio between the distance between electrodes (5 mm) and the value of the cross section area (YSZ layer thickness x 5 mm contacts width). This choice is justified by the negligible contribution of the STO to the total conductance (see below).

To evaluate a possible electronic contribution to the alternating current (ac) conductance of the samples, we have measured direct current (dc) conductance by using a dc technique. The measurements have been done with a constant voltage method by using a Keithley 6514 electrometer as pico-ampermeter and a Keithley 2400 source-meter as voltage source with an applied voltage signal of 100 mV. A guard electrode has been used, to prevent current leakages through the experimental set-up which allows measurement of currents down to 10^{-13} A. To better compare the dc conductance results obtained by ac and dc techniques, we have kept the same electrodes configuration in both measurements. In figure S2 we have plotted both quantities together (dc conductance obtained by ac and dc methods) together for a heterostructure with 1 nm YSZ layer sandwiched between 10 nm STO layers as a function of temperature. As can be observed in this figure, the dc conductance (open circles) is three to four orders of magnitude lower than the values obtained from ac measurements (solid squares) in the whole temperature measurement range. This result indicates that the electronic contribution to the ac measurements can be considered negligible and thus the measured ac transport is due to an ionic diffusion process. In addition, we also grew 10 nm STO films on single crystal YSZ substrates. The conductance values of these samples were the same as that of plain YSZ single crystals substrates and several orders of magnitude smaller than the conductance values found for the trilayer samples (see figure S2). In order to further dismiss any possible contribution of the STO substrate to the measured conductance we also measured the electrical conductance of an STO substrate by using the same geometrical configuration for the electrodes, which yielded a negligible value (always lower than the resolution limit of our measurements, 10^{-9} S, in the whole temperature range) compared to that measured in STO/YSZ/STO trilayers. Similar low

conductance values were obtained for 10 nm STO films grown on STO. Thus conduction through the STO cannot account for the high conductivity of the trilayers.

SOM TEXT

The conductivity pre-exponential factors of trilayers, taking values of about 10^7 $(\Omega\ cm)^{-1}$ as estimated from figure 3, are about 2 orders of magnitude larger than in the single crystal samples ($>10^4$ $(\Omega\ cm)^{-1}$). However, we would like to point out that these values are not unphysical. According to the widely accepted expression for the conductivity pre-exponential factor,

$$\sigma_\infty = \frac{4\alpha e^2 a^2 v_0 N e^{S/k_B}}{k_B T}$$

such difference could be justified in terms of both an increase in the concentration of oxygen vacancies (N), and of a larger entropy term ($\exp(S/k_B)$) due to an increased number of the possible configurations of available positions for the oxygen ions (enhanced positional disorder for the oxygen vacancies). In the previous expression α is a geometrical factor, a is the jump distance, ν_0 is the attempt frequency, e the electron charge and k_B the Boltzmann constant. Moreover, the values of the pre-exponential factor of about 10^7 $(\Omega\ cm)^{-1}$ are comparable to those found in other ion conductors such as β-AgI which shows a value of the pre-exponential factor of 10^8 $(\Omega\ cm)^{-1}$ (S3).

Finally, figure S3 shows the O K edge from an epitaxially strained 1 nm thick YSZ layer in a $[YSZ_{1nm}/STO_{10nm}]_9$ superlattice (red) and the O K edge from a thick, relaxed YSZ layer, comparable to reported bulk spectra in reference S4 (black). Noticeable changes in the fine structure are observed, consistent with significant structural distortions characteristic of a more cubic environment in the strained sample (S4).

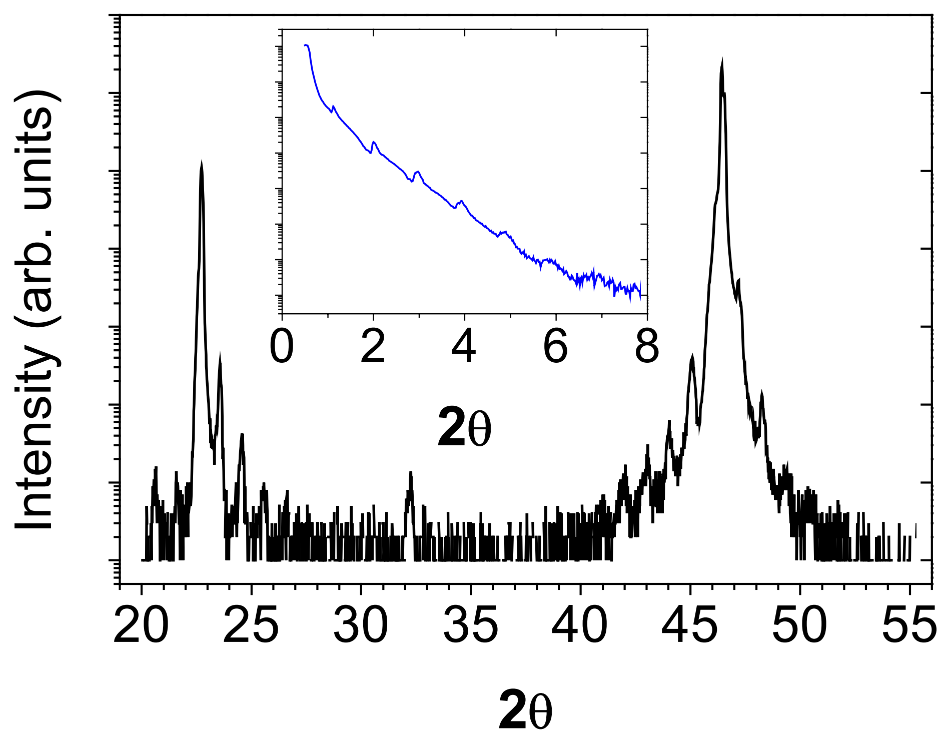

Figure S1. High angle (θ -2θ) XRD pattern of the $[YSZ_{1nm}/STO_{10\ nm}]_{20}$ superlattice**.** The inset shows the low angle reflectivity spectra of this sample.

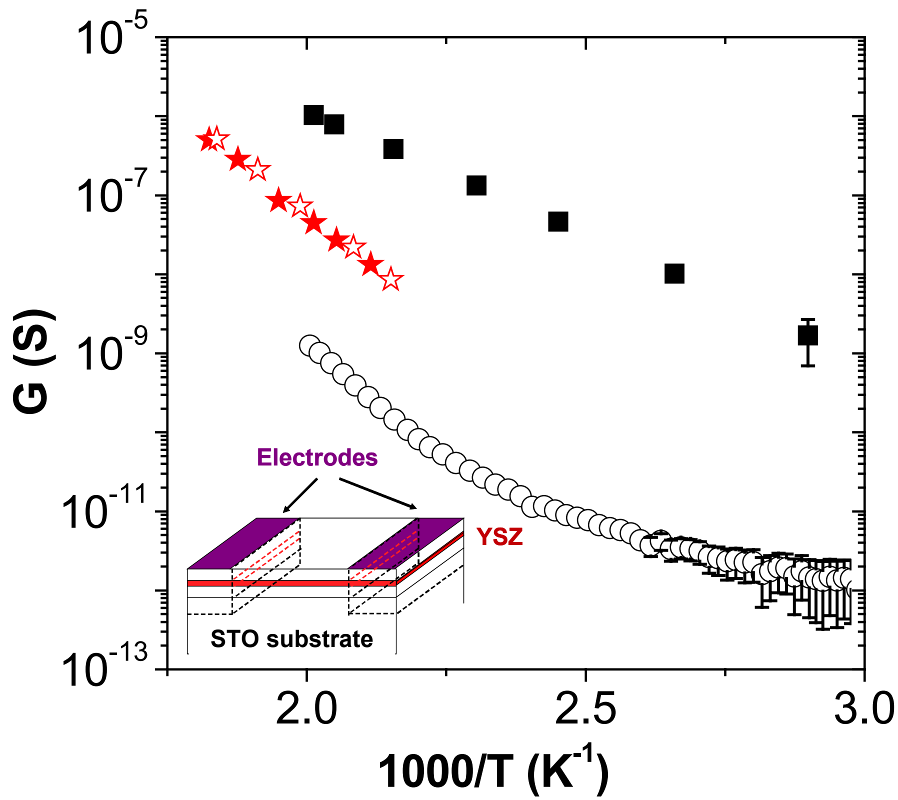

Figure S2. Arrhenius plot of the dc conductance, G, in Siemens (S) of the sample with a 1 nm thick YSZ layer sandwiched between 10 nm STO layers obtained by direct current (dc) (open circles) and alternating current (ac) (solid squares) measurements. Note that the uncertainty for conductance dc measurements is 10^{-12} S and 10^{-9} S for alternating current measurements. Solid stars: ac conductance of STO (10nm) layers grown on YSZ substrate. Open stars: ac conductance of a bare YSZ substrate with the same contact geometry. Inset: schematic illustration of the contact geometry in the lateral conductivity experiment. Dotted lines mark the contact geometry in the case of photolithographically buried contacts.

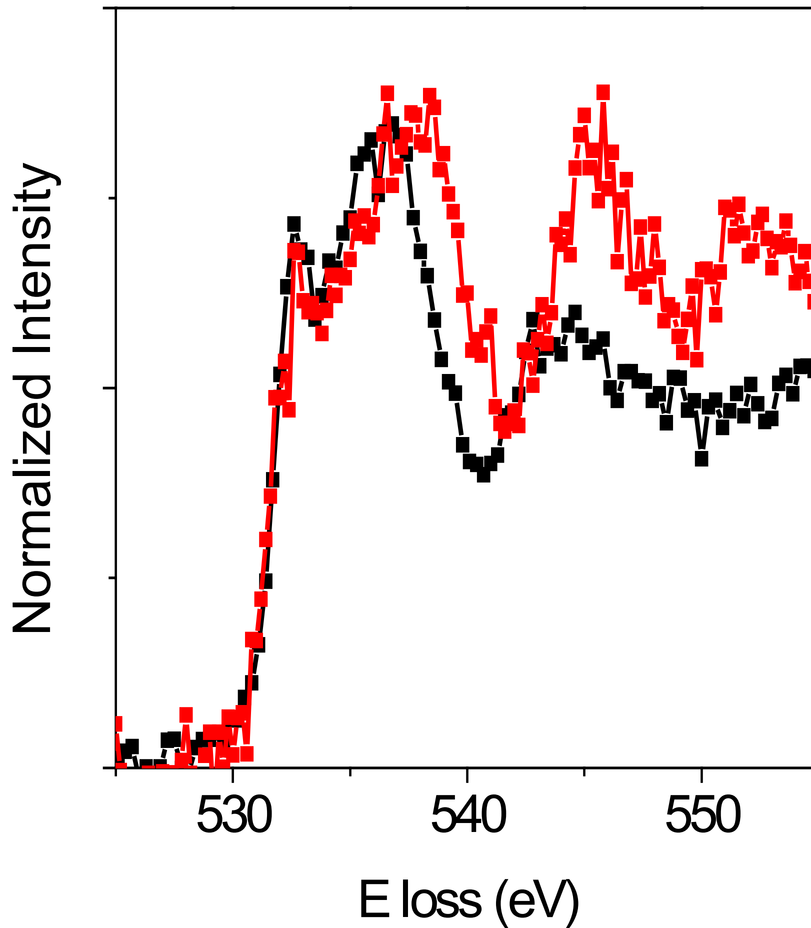

Figure S3. O K edge spectrum from a 1 nm thick YSZ layer in a $[YSZ_{1nm}/STO_{10\ nm}]_9$ superlattice (in red) and O K edge from a thick YSZ layer (black).

.

REFERENCES

S1. M. Varela, W. Grogger, D. Arias, Z. Sefrioui, C. Leon, C. Ballesteros, K. M. Krishnan, and J. Santamaria, Phys. Rev. Lett. **86**, 5156 (2001).

S2. V. Peña, Z. Sefrioui, D. Arias, C. Leon, J. Santamaria, J. L. Martinez, S. G. E. te Velthuis, and A. Hoffmann. Phys. Rev. Lett. **94**, 57002 (2005)

S3. R. J. Cava, E. A. Rietman, Phys. Rev. B **30**, 6896 (1984)

S4. S. Ostanin, A. J. Craven, D. W. McComb, D. Vlachos, A. Alavi, M. W. Finnis, A. T. Paxton. Phys. Rev. B **62**, 14728 (2000)